Adaptative Multigrid and Variable Parameterization for Optical-flow Estimation

Etienne Mémin, Patrick Pérez

INRIA
INSTITUT NATIONAL DE RECHERCHE EN INFORMATIQUE ET EN AUTOMATIQUE

Adaptative Multigrid and Variable Parameterization for Optical-flow Estimation

Etienne Mémin and Patrick Pérez

N° 3102

Janvier 1997

THÈME 3

ISSN 0249-6399

INRIA
RENNES

Adaptative Multigrid and Variable Parameterization for Optical-flow Estimation

Etienne Mémin and Patrick Pérez

Thème 3 — Interaction homme-machine,
images, données, connaissances
Projet TEMIS

Rapport de recherche n°3102 — Janvier 1997 — 19 pages

Abstract: We investigate the use of adaptative multigrid minimization algorithms for the estimation of the apparent motion field. The proposed approach provides a coherent and efficient framework for estimating piecewise smooth flow fields for different parameterizations relative to adaptative partitions of the image. The performances of the resulting algorithms are demonstrated in the difficult context of a non convex global energy formulation.

Key-words: optic flow, robust statistics, global minimization, adaptative grids, multigrid algorithms, variable parameterization

(Résumé : tsvp)

Algorithme multigrille adaptatif et paramétrisation variable pour l'estimation du flot optique

Résumé : Nous présentons une famille d'algorithmes de minimisation, multigrilles et adaptatifs, dédiés à l'estimation du champs des vitesses apparentes dans une séquence d'images. Ce schéma de minimisation est décrit de manière générale pour différentes paramétrisations du champ des vitesses. La formulation unifiée ainsi obtenue conduit de façon naturelle et cohérente à estimer sur une partition adaptée de l'image un champ comme fonction continue par morceaux avec divers degrés concomittants de paramétrage.

Mots-clé : flot optique, statistique robuste, minimisation globale, grilles adaptatives, algorithmes multigrilles, paramétrisation variable

1 Introduction

Energy-based models constitute a powerful way to cope with low-level image processing problems. Those methods are issued either from continuous formalisms such as PDEs or either from discrete modelization such as Markov random fields. The underlying problems are easily tractable if the energy is convex. One has then to deal with functions having an unique minimum that may be estimated with deterministic descent minimization algorithms. However, when it comes to design accurate and robust methods, able to handle and to locate as precisely as possible discontinuities, energies tend to be non linear with numerous local minima. The optical flow estimation is not an exception to this rule [5, 9, 10, 19, 21, 25]. Even within an incremental *multiresolution* formulation of the problem (which is almost inescapable in case of long range motions to be estimated), one has to deal with a sequence of global optimization problems which remain tricky.

To cope efficiently with such global energy minimization, we propose here a family of deterministic optimization algorithms. These *multigrid* algorithms are extensions of the method proposed in [21]. They allow to properly combine a multigrid minimization strategy with the mutiresolution framework commonly used in motion analysis. The key idea consists in the minimization of the energy function through an appropriate hierarchy of subspaces of the whole configuration space. Each subspace is defined as a set of configurations constrained to be piecewise parametric relative to a certain partition of the image.

These multigrid minimization algorithms turn out to provide an accelerated convergence toward improved estimates. Furthermore, associated to a dense robust optic flow estimation model, the multigrid framework provides efficient motion estimators allowing to combine different parameterizations of the velocity field through an adaptative partition of the image grid. A compromise solutions between local dense methods [5, 16, 21] involving smothness constraints and global parametric approaches assuming low order polynomial representation of the velocity field [1, 2, 4, 7] is thus introduced.

The remainder of the paper is organized as follows. In section 2, we present the robust motion estimation framework of interest. The estimation is presented as the incremental minimization of a global energy function. The objective function considered here, involves robust estimators to deal both with spatial discontinuities of the velocity field and with large deviations from the data model. In section 3, we present the proposed multigrid framework. Our approach is validated qualitatively and quantitatively on real world and synthetic sequences. These experimental results are reported in section 4.

2 Robust incremental estimation

Standard optical-flow estimators are based on the well known *optical flow constraint* (OFC) equation [16]. This differential equation, issued from a linearization of the brightness constancy assumption, links

the spatio-temporal gradients of the luminance to the unknown velocity vector. In order to estimate the two components of the velocity vector, a *smoothness* prior on the solution is usually combined with it through regularization [5, 14, 16].

Due to the differential nature of the OFC, this standard modeling does not hold for large displacements. To circumvent the problem, we consider an incremental estimation of the flow field captured both by the optic-flow multiresolution setup [5, 11, 14] and by the multigrid strategy *used at each resolution level* [15, 21]. The multiresolution framework involving a pyramidal decomposition of the image data is standard and won't be emphasized herein. In the following, we shall assume to work at a given resolution of this structure. However, one has to keep in mind that the expression and computations are meant to be reproduced at each resolution level according to a coarse to fine strategy.

Let us now assume that a rough estimate $\boldsymbol{w} = \{\boldsymbol{w}_s, s \in S\}$ of the unknown velocity field is available (e.g., from an estimation at lower resolution or from a previous estimation), on the rectangular pixel lattice S. Let $f(t) = \{f(s,t), s \in S\}$ be the luminance function at time t. Under the constancy brightness assumption from time t to $t+1$, a small *increment field* $\mathsf{d}\boldsymbol{w} \in \Omega \subset (\mathbb{R}\times\mathbb{R})^S$ can be estimated by minimizing the functional $H \triangleq H_1 + \alpha H_2$, with [5, 21]:

$$H_1(\mathsf{d}\boldsymbol{w}; f, \boldsymbol{w}) \triangleq \sum_{s\in S} \rho_1[\boldsymbol{\nabla} f(s+\boldsymbol{w}_s, t+1)^T \mathsf{d}\boldsymbol{w}_s + f_t(s,t,\boldsymbol{w}_s)\ ], \tag{1}$$

$$H_2(\mathsf{d}\boldsymbol{w}; f, \boldsymbol{w}) \triangleq \sum_{<s,r>\in\mathcal{C}} \rho_2\left[\|(\boldsymbol{w}_s + \mathsf{d}\boldsymbol{w}_s) - (\boldsymbol{w}_r + \mathsf{d}\boldsymbol{w}_r)\|\right], \tag{2}$$

where $\alpha > 0$, $\mathcal{C}$ is the set of neighboring site pairs lying on grid S equipped with some neighborhood system ν, $\boldsymbol{\nabla} f$ stands for the spatial gradient of f, $f_t(s,t,w_s) \triangleq f(s+\boldsymbol{w}_s, t+1) - f(s,t)$ is the displaced frame difference, and functions ρ_1 and ρ_2 are standard *robust M-estimators* (with hyper-parameters σ_1 and σ_2). Embedded into a *multiresolution coarse-to-fine* strategy, this incremental approach allows to estimate *large* velocities. Functions ρ_1 and ρ_2 penalize the *deviations* from the data model (i.e., the OFC) and from the first order smoothing prior, which are very likely to occur (e.g., especially around *occlusions*).

Roughly speaking, a robust M-estimator function ρ is an increasing cost which penalizes large "residual" values less drastically than quadratic functions do [6, 12, 8]. It can be shown that under certain simple conditions (mainly concavity of $\phi(v) \triangleq \rho(\sqrt{v})$), any multidimensional minimization problem of the form "find $\arg\min_x \sum_i \rho[g_i(x)]$" can be turned into a dual minimization problem "find $\arg\min_{x,z} \sum_i [m z_i g_i(x)^2 + \psi(z_i)]$" involving *auxiliary variables* (or *weights*) z_is continuously lying in $(0,1]$. ψ is a continuously differentiable function, depending on ρ, and $m \triangleq \lim_{v\to 0+} \phi'(v)$. The new minimization is then lead *alternatively* with respect to x and to the z_is. If g_is are affine forms, minimization w.r.t. x is a standard *weighted least squares* problem. In turn x being frozen, the best weights have the following closed form:

$$\hat{z}_i(x) = \frac{\rho'[g_i(x)]}{2 m g_i(x)} = \frac{1}{m}\phi'[g_i(x)^2]. \tag{3}$$

In our case the weights are of two natures: (a) *data outliers weights* (related to the dual formulation of H_1), and (b) *discontinuity weights* lying on the dual grid of S (provided by the dual formulation of H_2). The first set of weights, denoted by $\delta = \{\delta_s, s \in S\}$, allows to attenuate the effect of data for which the OFC is violated. The second one, denoted by $\beta = \{\beta_{sr}, <s,r> \in \mathcal{C}\}$, prevents from over-smoothing in locations obviously exhibiting significant velocity discontinuities. The estimation is now expressed as the global minimization in $(\mathtt{d}\boldsymbol{w}, \delta, \beta)$ of $\mathcal{H} \triangleq \mathcal{H}_1 + \alpha\mathcal{H}_2$ where:

$$\mathcal{H}_1(\mathtt{d}\boldsymbol{w}, \delta, \beta; f, w) = \sum_{s \in S} \left[m_1 \delta_s \left[\boldsymbol{\nabla} f(s+\boldsymbol{w}_s, t+1)^T \mathtt{d}\boldsymbol{w}_s + f_t(s, t, \boldsymbol{w}_s) \right]^2 + \psi_1(\delta_s) \right], \tag{4}$$

$$\mathcal{H}_2(\mathtt{d}\boldsymbol{w}, \delta, \beta; f, w) = \sum_{<s,r> \in \mathcal{C}} \left[m_2 \beta_{sr} \|(\boldsymbol{w}_s + \mathtt{d}\boldsymbol{w}_s) - (\boldsymbol{w}_r + \mathtt{d}\boldsymbol{w}_r)\|^2 + \psi_2(\beta_{sr}) \right]. \tag{5}$$

However, the underlying energy function H being non-convex with respect to the unknown variables of interest, we still have to deal with a tough optimization problem, in spite of the reformulation. In particular, the alternate minimization procedure is not guaranteed to reach a global minimum, even though each step is constituted of an exact minimization (but with respect to only a subset of variables).

3 Multigrid minimization

To efficiently cope with our global optimization problem, we design a hierarchical "constrained" exploration of the configuration space Ω: the optimization is lead through a sequence of constrained configuration subspaces of increasing size

$$\dim(\Omega^L) < \dim(\Omega^{L-1}) < \cdots < \dim(\Omega^0) \text{ with } \Omega^0 = \Omega, \tag{6}$$

and where Ω^ℓ is the set of increment fields which are constrained to be piecewise parametric according to a partition of grid S. Let $\mathcal{B}^\ell \triangleq \{\mathcal{B}_n^\ell,\ n = 1, \ldots, N_\ell\}$ denotes this partition and S^ℓ the vertices of the associated connectivity graph[1]. Each patch of the incremental field is defined such as:

$$\forall n \in S^\ell,\ \forall s \in \mathcal{B}_n^\ell,\ \mathtt{d}\boldsymbol{w}_s = \Phi_n^\ell(\boldsymbol{\Theta}_n^\ell, s), \tag{7}$$

where $\boldsymbol{\Theta}_n^\ell$ is a parameter vector. The whole increment can then be expressed:

$$\mathtt{d}\boldsymbol{w} = \Phi^\ell(\boldsymbol{\Theta}^\ell), \tag{8}$$

with $\boldsymbol{\Theta}^\ell = \{\boldsymbol{\Theta}_n^\ell, n \in S^\ell\}$ lying in the reduced parameter space Γ^ℓ. The full-rank function Φ^ℓ is the *interpolation operator* between the reduced subspace Γ^ℓ and the full original configuration space Ω. It is a one-to-one mapping from Γ^ℓ into $\Omega^\ell = \mathrm{Im}\Phi^\ell$.

[1] Let us note that in case of a regular square block partition $\mathcal{B}^\ell$, the graph S^ℓ is a N_ℓ-site rectangular grid.

3.1 Different parameterizations and their mixing

In this work we focus on linear forms of the interpolation operator:

$$\forall n \in S^\ell, \forall s \in \mathcal{B}_n^\ell, \mathsf{d}\boldsymbol{w}_s = P_n(s)\boldsymbol{\Theta}_n^\ell, \tag{9}$$

where $P_n(s)$ is 2 by p_n matrix. The corresponding parameter spaces are in these cases $\Gamma^\ell = \mathbb{R}^{p_1} \times \cdots \times \mathbb{R}^{p_{N_\ell}}$. The standard parametric models used in motion analysis correspond to p_n=2, 4, 6 or 8 [1, 4]. In this work we will consider three different parameterizations of the configuration subspaces (in the following x stands for the vertical axis whereas y denotes the horizontal one, the origin point being the upper left corner of grid S, in this form, x_s and y_s are the coordinates of sites s).

Blockwise constant model

Here, the configuration of Ω^ℓ are constrained to be piecewise constant over each patch of the partition $\mathcal{B}^\ell$:

$$\forall n \in S^\ell, \forall s \in \mathcal{B}_n^\ell, P_n(s) = \begin{bmatrix} 1 & 0 \\ 0 & 1 \end{bmatrix} \triangleq \mathbb{I}_2, \text{i.e., } \mathsf{d}\boldsymbol{w}_s = \boldsymbol{\Theta}_n^\ell = \begin{bmatrix} \mathsf{d}u_n^\ell \\ \mathsf{d}v_n^\ell \end{bmatrix} \tag{10}$$

This kind of constraint has been extensively used in a regularization-free context of conventional block-matching techniques for video coding. It has also been successfully used for the design of multigrid models with regularization, for motion estimation and segmentation (both in motion analysis [21] and video coding [23]). Despite its simplicity, this constraint gives fast and excellent results [21, 24].

Piecewise simplified affine model

In this second model the projection between the subspaces Γ^ℓ and the configuration space Ω^ℓ is described by a four parameters transformation:

$$\forall n \in S^\ell,\ \forall s \in \mathcal{B}_n^\ell,\ P_n(s) = \begin{bmatrix} 1 & 0 & x_s & y_s \\ 0 & 1 & y_s & -x_s \end{bmatrix} \text{ and } \boldsymbol{\Theta}_n^\ell = \begin{bmatrix} tx_n^\ell & ty_n^\ell & div_n^\ell & curl_n^\ell \end{bmatrix}^T. \tag{11}$$

This model conjectures that the partition patches correspond to the projection of 3D planar facets parallel to the image plane with apparent motion restricted to translation, divergence and rotation. It is known as the simplified affine model.

Piecewise affine model

Usually a more complete affine model is preferred. Here the 3D planar patches of surface are not anymore supposed to be parallel to the image plane and their motions are confined to rotations around

the optical axis and to translation in the facet's plan. The constraint is described by a six parameters vector:

$$\forall n \in S^\ell, \forall s \in \mathcal{B}_n^\ell,\ P_n(s) = \begin{bmatrix} 1 & x_s & y_s & 0 & 0 & 0 \\ 0 & 0 & 0 & 1 & x_s & y_s \end{bmatrix} \text{ and } \mathbf{\Theta}_n^\ell = \begin{bmatrix} a_n^\ell & b_n^\ell & c_n^\ell & d_n^\ell & e_n^\ell & f_n^\ell \end{bmatrix}^T. \tag{12}$$

The affine model has been widely used for motion-based segmentation [1, 2, 7] or for the estimation of dominant motion over the entire image [5, 17, 22]. It is considered as a good trade off between model complexity and model efficiency [7]. In segmentation applications, the affine model defines the profile of the flow inside each segment of the associated image partition. The accuracy of the field estimation depends obviously on the quality of the segmentation. If the considered regions are too large then a single affine model may badly represents the motion of the associated 3D surface. The planarity hypothesis are indeed very likely to be violated in this case. On the opposite, since usually no "continuity" between patches is maintained on the velocity field, smaller regions may lead to inaccurate motion estimation. This inaccuracy occurs if the linear system to be solved is badly conditioned (in regions having uniform luminance for example or in areas, such as occlusion regions, where the OFC is not valid at all). Recently, a blockwise smooth parametric model involving inter-block regularization has been considered [18]. In this work, the field is constrained to be locally affine on a block partition and a regularization term in the parameter space is added in order to enforce smoothness across patches. However, the regularization prior considered does not allow to easily support different parameterizations of the flow field. Furthermore, this approach is not defined hierarchically and thus implies to consider mixture of models when the block involves several motions or a complex motion profile. The unknown number of mixtures components has to be estimated with an EM-type algorithm or some of its variants [2].

3.2 Multigrid energy derivation

Let us now see more precisely how these different parametric models may be embedded within an unified hierarchical minimization scheme over constrained configurations subspaces Ω^ℓ. Recalling that our purpose is to build a hierarchy of such subspaces the partitions have to satisfy the following property:

$$\forall n \in S^\ell, \exists\,!\ \bar{n} \in S^{\ell+1} :\ \mathcal{B}_n^\ell \subset \mathcal{B}_{\bar{n}}^{\ell+1}, \tag{13}$$

which expresses that $\mathcal{B}^\ell$ corresponds to a subdivision of elements of $\mathcal{B}^{\ell+1}$. This induces a natural tree structure for which $\bar{n}$ is the parent of n.

The constrained optimization in $\Omega^\ell = \mathrm{Im}\Phi^\ell$ is obviously equivalent to the minimization of the new energy function:

$$\mathcal{H}^\ell(\mathbf{\Theta}^\ell, \delta, \beta; f, \boldsymbol{w}) \triangleq \mathcal{H}(\Phi^\ell(\mathbf{\Theta}^\ell), \delta, \beta; f, \boldsymbol{w}),$$

defined over Γ^ℓ, whereas the weights, the data, and the field to be refined remain the same (i.e., defined on the original grid S). From this family of energy functions, we are now able to define our minimization scheme as a cascade (from $\ell = L$ to $\ell = 0$) of optimization problems of reduced complexity:

$$(\hat{\mathbf{\Theta}}^\ell, \hat{\delta}, \hat{\beta}) = \arg\min_{\mathbf{\Theta}^\ell, \delta, \beta} \mathcal{H}^\ell(\mathbf{\Theta}^\ell, \delta, \beta; f, \underbrace{\boldsymbol{w}^{\ell+1} + \Phi^{\ell+1}(\hat{\mathbf{\Theta}}^{\ell+1})}_{\boldsymbol{w}^\ell}), \ \ell = L, \ldots, 0, \tag{14}$$

with $\hat{\mathbf{\Theta}}^{\ell+1} \equiv 0$. The field $\mathbf{\Theta}^\ell \in \Gamma^\ell$ lies on the reduced grid S^ℓ whereas the weights and the main velocity components, $\boldsymbol{w}^\ell \triangleq \boldsymbol{w}^{\ell+1} + \Phi^{\ell+1}(\hat{\mathbf{\Theta}}^{\ell+1})$, are attached to S, whatever the grid level ℓ. The initial field $\boldsymbol{w}^\ell = \boldsymbol{w}^{L+1} = \boldsymbol{w}$ comes from an estimation at a coarser resolution or from a given initialization.

Each of these successive minimizations are processed in terms of iteratively reweighted least squares and a multigrid coarse-to-fine strategy is developed: the increment field estimated at level $\ell + 1$, $\Phi^{\ell+1}(\mathtt{d}\boldsymbol{w}^{\ell+1})$ is added to $\boldsymbol{w}^{\ell+1}$ to form the new main component of the velocity field $\boldsymbol{w}^\ell$, $f(t)$ is warped accordingly for the computation of the spatial and temporal derivatives and a new increment is then estimated at level ℓ. This procedure is repeated until the finest level $\ell = 0$ is reached.

The new multigrid energy functions[2] $\mathcal{H}^\ell$ may be easily derived from the original one (4-5). They are also composed of two terms $\mathcal{H}^\ell = \mathcal{H}_1^\ell + \alpha\mathcal{H}_2^\ell$ where $\mathcal{H}_1^\ell$ and $\mathcal{H}_2^\ell$ are respectively:

$$\mathcal{H}_1^\ell = \sum_{n \in S^\ell} \sum_{s \in \mathcal{B}_n^\ell} m_1 \delta_s \left[\boldsymbol{\nabla} f(s + \boldsymbol{w}_s^\ell, t+1)^T P_n(s) \mathbf{\Theta}_n^\ell + f_t(s, t, \boldsymbol{w}_s^\ell) \right]^2 + \psi_1(\delta_s) \tag{15}$$

and

$$\begin{aligned} \mathcal{H}_2^\ell = & \sum_{<n,m> \in \mathcal{C}^\ell} \sum_{<s,r> \in \mathcal{C}_{nm}^\ell} m_2 \beta_{sr} \left\| (\boldsymbol{w}_s^\ell + P_n(s)\mathbf{\Theta}_n^\ell) - (\boldsymbol{w}_r^\ell + P_m(r)\mathbf{\Theta}_m^\ell) \right\|^2 + \psi_2(\beta_{sr}) + \\ & \sum_{n \in S^\ell} \sum_{<s,r> \in \mathcal{C}_n^\ell} m_3 \beta_{sr} \left\| (\boldsymbol{w}_s^\ell + P_n(s)\mathbf{\Theta}_n^\ell) - (\boldsymbol{w}_r^\ell + P_n(r)\mathbf{\Theta}_n^\ell) \right\|^2 + \psi_2(\beta_{sr}) \end{aligned} \tag{16}$$

where $\mathcal{C}_n^\ell \triangleq \{<s,r> \in \mathcal{C} : <s,r> \subset \mathcal{B}_n^\ell\}$ is the set of neighboring site pairs included in patch $\mathcal{B}_n^\ell$ and $\mathcal{C}_{nm}^\ell \triangleq \{<s,r> \in \mathcal{C} : s \in \mathcal{B}_n^\ell, r \in \mathcal{B}_m^\ell\}$ the set of neighboring site pairs straddling $\mathcal{B}_n^\ell$ and $\mathcal{B}_m^\ell$. All possible $\mathcal{C}_n^\ell$ and $\mathcal{C}_{nm}^\ell$ site sets form a partition of $\mathcal{C}$. Reduced site set S^ℓ turns out to be equipped with a new neighborhood system ν^ℓ [3]. The corresponding neighboring pair set will be denoted by $\mathcal{C}^\ell$. In $\mathcal{H}_2$, we consider different hyper-parameter values, m_2 and m_3, depending on whether the site pairs are inside a patch or straddling its border. A low value of this hyper-parameter inside each patch (i.e., a reduced regularization) will allow us to favor a larger class of affine motion increments inside each block since all the variables are then almost decorrelated. The last term of $\mathcal{H}_2$ can thus be made negligible.

[2] We use here the dual form of M-estimators. This could as well be described in their initial formulation.

[3] In case of regular partition with $2^\ell \times 2^\ell$ blocks, ν^ℓ turns out to be the same neighborhood system as the original one ν (see [15]).

3.3 Energy minimization

The current reduced parameter estimate $\hat{\mathbf{\Theta}}^\ell$ being fixed, we know that the optimal weight values are directly accessible. According to (3), in combination with energy definitions (15-16), these values are:

$$\bullet \forall s \in \mathcal{B}_n^\ell, \hat{\delta}_s = \frac{1}{m_1}\phi_1' \left[\left(\nabla f(s+\boldsymbol{w}_s^\ell, t+1)^T P_n(s) \hat{\mathbf{\Theta}}_n^\ell + f_t(s,t,\boldsymbol{w}_s^\ell) \right)^2 \right], \tag{17}$$

$$\bullet \forall <s,r> \in \mathcal{C}_{nm}^\ell,\ \hat{\beta}_{sr} = \frac{1}{m_2}\phi_2' \left[\left\| (\boldsymbol{w}_s^\ell + P_n(s)\hat{\mathbf{\Theta}}_n^\ell) - (\boldsymbol{w}_r^\ell + P_n(r)\hat{\mathbf{\Theta}}_m^\ell) \right\|^2 \right], \tag{18}$$

$$\bullet \forall <s,r> \in \mathcal{C}_n^\ell,\ \hat{\beta}_{sr} = \frac{1}{m_3}\phi_2' \left[\left\| \boldsymbol{w}_s^\ell - \boldsymbol{w}_r^\ell + (P_n(s) - P_n(r))\hat{\mathbf{\Theta}}_n^\ell \right\|^2 \right]. \tag{19}$$

It is worth noting that according to (19), the discontinuity variables β_{sr} located into patches of $\mathcal{B}^\ell$ (i.e., $<s,r> \in \mathcal{C}_n^\ell$ for some $n \in S^\ell$) do not depend on translational components of $\mathbf{\Theta}$. In the *piecewise constant* case they therefore only depend on $\boldsymbol{w}^\ell$. In such case, they can be computed right away at the first iteration at the current grid level. As soon as the values of weights are computed and frozen, the energy function $\mathcal{H}^\ell(\mathbf{\Theta}^\ell, \delta, \beta; f, \boldsymbol{w}^\ell)$ is quadratic with respect to $\mathbf{\Theta}^\ell$. Its minimization is equivalent to the resolution of a linear system whose solution is searched with an iterative Gauss-Seidel scheme. Each update is obtained by solving a linear equation in $\mathbf{\Theta}_n^\ell$ for the current block $\mathcal{B}_n^\ell$. This equation is detailed in the Appendix for the three different possible parameterizations of $\mathtt{d}\boldsymbol{w}$ on $\mathcal{B}_n^\ell$.

3.4 Adaptative grids

The different parametric models previously presented do not imply the same computational load. Furthermore, they are different in terms of locality and accuracy. For example the six parameter affine model allows to describe the global motion profile of large areas whereas the constant model is accurate only for small patches. In order to better fit the content of the image, it seems interesting to mix different levels of parameterization along with an adapted partionning. Such an adaptative structure must be able to remain coarse grain on region where the flow field may be approximate with a good accuracy on the basis of a general parametric model (i.e., six or four parameter affine model). If the motion of a region cannot be satisfactory described that way, then the description should be locally refined with a more accurate model lying on a finer subdivision of the region. Such adaptative grids are considered in [26] where a blockwise parametric motion model (a spline based description) is locally refined on smaller blocks if the mean square error between frame (t) and the frame $(t+1)$ backward registered exceeds a certain threshold. However this approach does not make use of regularization. A different approach based on finite elements method considers a threshold on the normal flow field (which are directly accessible from the OFC) [9]. In this case the computation of the adaptative grid is done *a priori*. Our robust incremental motion model permits to directly have access to such information through the data auxiliary variables [4] and to use it on line. We consider an adaptative grid structure

[4] More precisely, they account for the linearized errors between the frame $(t+1)$ backward registered and frame (t).

relying on the following subdivision criterion: at convergence on the current grid level, a patch is split in four parts if the standard deviation of the data outliers on that patch is greater than a certain threshold.

4 Experimental results

In this section we present results obtained both on synthetic and real-world sequences. The first sequence, Yosemite, is the most complex (though synthetic) sequence from the comparative study by Barron *et al.* [3] for which a "ground-truth" exists. The second test sequence named Affine-meteo, have been obtained by applying a complex motion field composed of a spatial linear combination of five 6-parameter affine motion on a real image (Fig. 3a). This synthetic benchmark is a difficult example since the different moving regions create large motion discontinuities (Fig. 1).

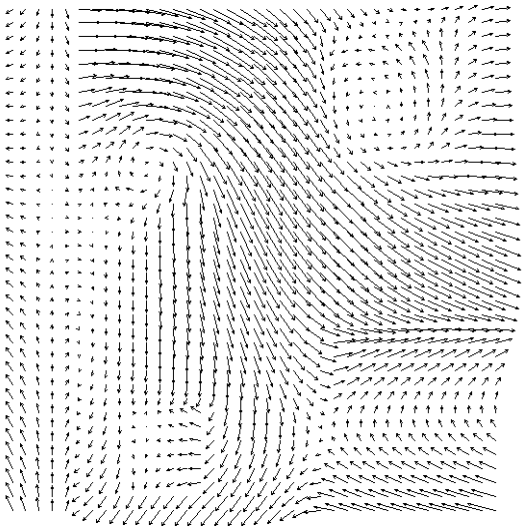

Figure 1: Synthetic motion field

The third one named Depression (Fig. 3a) is a meteorological sequence involving large displacements. It includes a through of low pressure and some moving clouds driven by different motions.

In our experiments we have tested different motion estimator arising from our approach. First of all, though our multigrid scheme being defined for any partition of the image, for sake of simplicity we will consider here only square block partitions. The multigrid framework has been evaluated for the three kinds of constraint previously described. This yields different *estimation models* which have been run both on *regular grids* and *adaptative grids*. In the first case, the multigrid minimization is associated to a regular and complete subdivision scheme leading to consider a single parametric class at every grid level. Whereas, in the second case we have to deal with irregular grids issued from the adaptative subdivision strategy described section 3.4 and where the type of parameterization on each patch may depend on its size.

	Yosemite	Affine-meteo	Depression
number of resolution levels $(N+1)$	2	2	3
number of grid levels at each resolution $(L+1)$	5	6	5
smoothing parameter α	320	50	200
parameters σ_1 tuning ρ_1	6	7	7
parameters σ_2 tuning ρ_2 inter blocks	0.7	0.1	0.3
parameters σ_3 tuning ρ_2 intra block	0.001	0.001	0.05

Table 1: Parameter values for experiments on the three sequences

The different estimation models are denoted $\mathcal{M}_{\mathbf{6}}$, $\mathcal{M}_{\mathbf{4}}$, $\mathcal{M}_{\mathbf{2}}$, $\mathcal{M}_{\mathbf{6,4}}$, $\mathcal{M}_{\mathbf{6,2}}$ and $\mathcal{M}_{\mathbf{6,4,2}}$. The first three concern respectively the 6-parameters affine models ($\mathcal{M}_{\mathbf{6}}$), the simplified affine model ($\mathcal{M}_{\mathbf{4}}$) and the constant model ($\mathcal{M}_{\mathbf{2}}$). The others are multi-parametric versions where several parameterizations are successively imposed (regular case) or mixed (adaptative case). $\mathcal{M}_{\mathbf{6,4}}$ associates the 6-parameters affine model and simplified affine model whereas $\mathcal{M}_{\mathbf{6,2}}$ involves constant model and affine model and finally $\mathcal{M}_{\mathbf{6,4,2}}$ includes the three models. The finest grid level (resp. the finest block size in case of adaptative grids) actually considered in the single parametric estimation model depends on the parameterization used. It is $\ell_0 = 3$ (8×8 blocks) for $\mathcal{M}_{\mathbf{6}}$, $\ell_0 = 2$ (4×4 blocks) for $\mathcal{M}_{\mathbf{4}}$, and $\ell_0 = 0$ for $\mathcal{M}_{\mathbf{2}}$. By contrast, the current parameterization to consider in the multi-parametric versions depends on the grid level (resp. the block size). We imposed to have the 6-parameter affine model in $\mathcal{M}_{\mathbf{6,4}}$, $\mathcal{M}_{\mathbf{6,2}}$ and $\mathcal{M}_{\mathbf{6,4,2}}$ if $\ell > 2$ (resp. $|\mathcal{B}_n^\ell| > 4 \times 4$). For $\mathcal{M}_{\mathbf{6,4}}$ and $\mathcal{M}_{\mathbf{6,4,2}}$ we used the simplified affine model if $\ell = 2$ (this level being the finest grid level for $\mathcal{M}_{\mathbf{6,4}}$). The constant model is involved if ℓ=1 or 0 for $\mathcal{M}_{\mathbf{6,4,2}}$ and if ℓ=2, 1 or 0 for $\mathcal{M}_{\mathbf{6,2}}$

We must outline that the different proposed algorithms were run with the same set of hyper-parameters (see Table 1).

The choice of the two robust estimators ρ_1 and ρ_2 has been based on heuristic considerations arising from our experience. Since frequent and large deviations from the brightness constancy assumption are more than likely to occur, a strongly saturating estimator seems to be well suited to the corresponding component of the energy function. We selected Leclerc's estimator [20] $\rho_1(u) \triangleq 1 - \exp(-u^2/\sigma_1^2)$ (see Fig. 2). On the contrary, a softer saturation (i.e., a slower decreasing rate of the estimator's derivative) seems to be better as far as regularization is concerned. We chose Geman and McClure's estimator [13]: $\rho_2(u) \triangleq \frac{u^2}{u^2+\sigma_2}$ (see Fig. 2).

Following [3], quantitative comparative results on Yosemite and on Affine-meteo are provided for different algorithms. For each estimate, angular deviations with respect to the real flow are computed at "reliable" locations (the percentage of such locations is the "density" of the estimate). In our case the proposed method yields always a full density. Table 2 and 4 list, for all the different algorithms

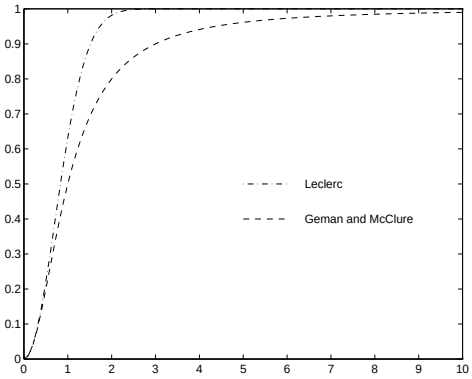

Figure 2: Leclerc's estimator and Geman-McClure's estimator.

Regular grids				Adaptive grids			
model	$\bar{\mu}$	σ	cpu	model	$\bar{\mu}$	σ	cpu
$\mathcal{M}_6$	5.07^o	7.20^o	34s	$\mathcal{M}_6$	5.09^o	7.20^o	28s
$\mathcal{M}_4$	5.56^o	9.20^o	72s	$\mathcal{M}_4$	6.57^o	9.20^o	58s
$\mathcal{M}_2$	4.97^o	7.64^o	64s	$\mathcal{M}_2$	6.53^o	7.64^o	42s
$\mathcal{M}_{6,4}$	5.01^o	7.23^o	58s	$\mathcal{M}_{6,4}$	5.17^o	7.62^o	44s
$\mathcal{M}_{6,2}$	4.69^o	6.89^o	78s	$\mathcal{M}_{6,2}$	5.25^o	7.87^o	72s
$\mathcal{M}_{6,4,2}$	4.75^o	6.89^o	92s	$\mathcal{M}_{6,4,2}$	5.31^o	7.86^o	73s

Table 2: Results on Yosemite

Technique	$\bar{\mu}$	σ	dens.
H. and S. (original)	31.69^o	31.18^o	100%
Horn and Shunck (modified)	9.78^o	16.19^o	100%
Uras *et al*	8.94^o	15.61^o	100%
Lucas and Kanade	4.28^o	11.41^o	35.1%
Fleet and Jepson	4.63^o	13.42^o	34.1%

Table 3: Comparative results on Yosemite

proposed here, the mean angular error ($\bar{\mu}$) and the associated standard deviation (σ). The CPU times, measured on a SUN ULTRA SPARC, are also reported in there.

The table 3 recalls some of the results presented by Barron *et al.* (see corresponding references therein). They concern an adaptation of Horn and Schunck's algorithm, the best full-density algorithm (Uras *et al.*) and the two algorithms yielding the best results, but besides, with reduced densities (Lucas and Kanade, Fleet and Jepson) [5]

[5] Other results on a sequence where the sky is removed is sometimes considered by other authors [5, 18, 21]. We believe that the resulting motion is probably too simple to yield significant differences between the different state-of-the-art motion estimators.

Regular grids				Adaptive grids			
model	$\bar{\mu}$	σ	cpu	model	$\bar{\mu}$	σ	cpu
$\mathcal{M}_6$	2.86^o	4.57^o	27s	$\mathcal{M}_6$	3.64^o	5.03^o	20s
$\mathcal{M}_4$	4.13^o	5.15^o	65s	$\mathcal{M}_4$	5.67^o	6.26^o	47s
$\mathcal{M}_2$	3.62^o	5.19^o	61s	$\mathcal{M}_2$	6.20^o	7.51^o	42s
$\mathcal{M}_{6,4}$	2.70^o	4.99^o	46s	$\mathcal{M}_{6,4}$	3.82^o	4.98^o	33s
$\mathcal{M}_{6,2}$	2.49^o	3.82^o	67s	$\mathcal{M}_{6,2}$	3.78^o	4.29^o	51s
$\mathcal{M}_{6,4,2}$	2.62^o	5.14^o	78s	$\mathcal{M}_{6,4,2}$	3.87^o	5.58^o	51s

Table 4: Results on Affine-meteo

On Yosemite sequence our methods associated to regular grids provide a *dense* estimate almost as good as those obtained with the best (non-dense) mentioned methods. Besides, except in the case of the simplified affine model, the standard deviation are significantly lowered.

On both sequences Yosemite and Affine-meteo, the best results are obtained for multiple parameterization models on regular grids. This is particularly noticeable when the three parametric models are associated or when the 6-parameters affine model is coupled with the constant model.

The $\mathcal{M}_6$ model on adaptative grids gives the lowest computation times. Compared to the other models on irregular grids, it also yields the best results. In particular, in that context multi-parametric models do not improved the results. At that point, let us remark that the comparison test developed by Barron *et al.* does not take really into account the ability of a method to detect more or less accurately the spatial discontinuities of the velocity field. It measures only an average deviation between the real flow field and the estimated one. As one would expect, the result of $\mathcal{M}_4$ and $\mathcal{M}_2$ on adaptative grids are very poor. These models have to be used with a regular subdivision strategy.

To complete our comparisons, we show results obtained on a real world sequence. Figure 3 presents for the atmospheric image Depression, the final velocity fields estimated by two different multigrid estimators. The first flow (Fig. 3c) is the final flow obtained by $\mathcal{M}_2$ on regular grids. The second one (Fig. 3d) has been produced by $\mathcal{M}_6$ on adaptative grid structure (the corresponding final grid is shown in figure 3d). The two flows are displayed the same way, namely subsampled by 6 and magnified by 4.

We can notice that with the constant constraint, the flow is drastically under-estimated compared to the one produced with the affine constraint. Besides, the blockwise constant multigrid yields in this case an over-smoothing of the solution. As a consequence on Depression, local features of interest such as the depression center in left upper corner of the image are concealed. This is not the case with affine modeling where the depression center is visible and may be easily identified in an automatic way.

Finally, note the whole multiresolution/multigrid algorithm converges quickly, since only ten or so low cost iterations are required at each grid level. Furthermore, as demonstrated in [21] for the constant model, the resulting motion estimator possesses a low sensitiveness to parameter's values.

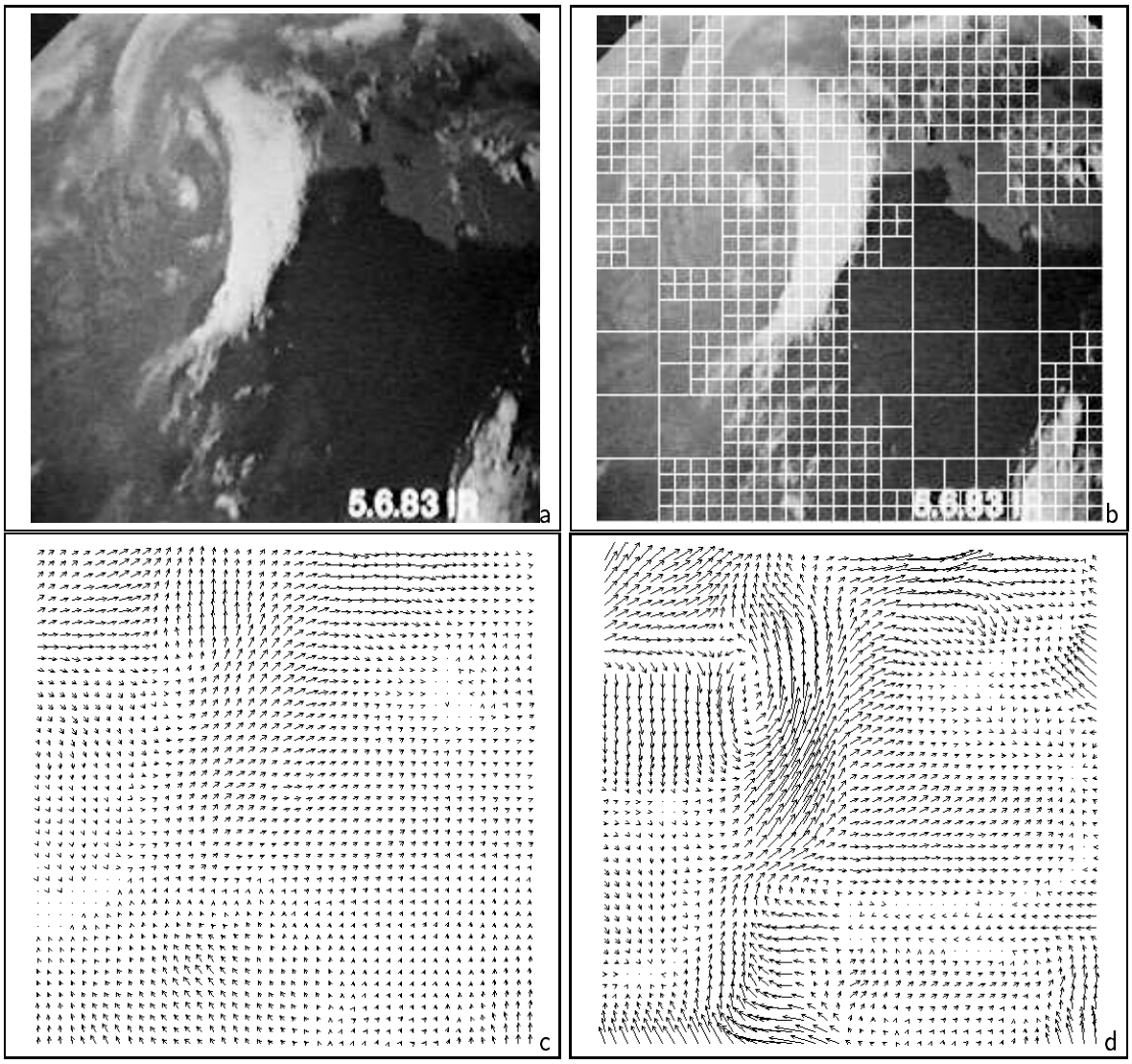

Figure 3: Results on Depression: (a) one frame, (b) final adaptative grid, (c) flow estimate with the constant regular multigrid algorithm (**cpu: 105s**), (d) flow estimate with the affine adaptative multigrid algorithm (**cpu: 24s**)

5 Conclusion

In this paper, we have presented a comprehensive multigrid framework for incremental optical flow estimation. The problem is expressed as the global minimization of an energy function which involves robust estimators to avoid spatial over-smoothing and to attenuate the influence of large deviations from the OFC. The minimization is efficiently performed through a multigrid algorithm which consists in imposing successively weaker and weaker constraints on the searched estimates. The formulation of this framework is general and allows to mix different parameterization levels of the flow field. Furthermore, it yields a unified and coherent description of an hierarchical motion estimators family which gives good results on sequences involving fluid or rigid motions [21]. Better results should even be obtained by driving the adaptative partition with an extra photometric criterion. This should allow a better estimation of the discontinuities and therefore provide more efficient schemes.

Appendix: Gauss-Seidel multigrid iteration for multiple parameterization on variable grid

For the sake of concision, we shall denote $\tilde{\boldsymbol{\nabla}} f(s) \triangleq \boldsymbol{\nabla} f(s + \boldsymbol{w}_s^\ell, t+1)$ the spatial gradient in the second image, displaced according to $\boldsymbol{w}^\ell$, and $\tilde{f}_t(s) = f_t(s, t, \boldsymbol{w}_s^\ell)$ the displaced frame difference. Now, if $\mathcal{B}_n$ is the current block in the iterative visit process implied by Gauss-Seidel method, one has simply to minimize $\mathcal{H}^\ell$ with respect to $\boldsymbol{\Theta}_n^\ell$, the total field outside $\mathcal{B}_s^\ell$ being frozen. The fraction of energy actually concerned is thus:

$$\begin{aligned}\mathcal{H}_n^\ell(\boldsymbol{\Theta}_n^\ell, \delta, \beta; f, \boldsymbol{w}) =& m_1 \sum_{s \in \mathcal{B}_n^\ell} \delta_s \left[\tilde{\boldsymbol{\nabla}} f(s)^T P_n(s) \boldsymbol{\Theta}_n^\ell + \tilde{f}_t(s)\right]^2 \\ &+ \alpha m_2 \sum_{<s,r> \in \mathcal{C}_{\partial n}^\ell} \beta_{sr} \left\| \boldsymbol{w}_s^\ell + P_n(s)\boldsymbol{\Theta}_n^\ell - \boldsymbol{w}_r \right\|^2 \\ &+ \alpha m_3 \sum_{<s,r> \in \mathcal{C}_n^\ell} \beta_{sr} \left\| (\boldsymbol{w}_s^\ell + P_n(s)\boldsymbol{\Theta}_n^\ell) - (\boldsymbol{w}_r^\ell + P_n(r)\boldsymbol{\Theta}_n^\ell) \right\|^2,\end{aligned} \tag{20}$$

where $\mathcal{C}_{\partial n}^\ell \triangleq \cup_{m \in \nu^\ell(n)} \mathcal{C}_{nm}^\ell$ is the set of cliques of $\mathcal{C}$ straddling the border of $\mathcal{B}_n^\ell$. The increment field on the neighboring sites of the block is defined by different parameterizations relative to different parts of the (possibly) irregular grid S^ℓ: for $m \in \nu^\ell(n)$ and $< s, r > \in \mathcal{C}_{nm}$, $\mathtt{d}\boldsymbol{w}_r = P_m(r)\boldsymbol{\Theta}_m^\ell$. However, the only thing of actual interest when updating $\boldsymbol{\Theta}_n^\ell$ is the total field $\boldsymbol{w}_r \triangleq \boldsymbol{w}_r^\ell + P_m(r)\boldsymbol{\Theta}_m^\ell$. As a consequence, in the following computations, the regularization is taken into account whatever the neighboring parameterizations are, thus allowing to simultaneously support different parametric models.

Writing that the partial derivative of this piece of energy vanishes, one gets:

$$\begin{aligned}\frac{\partial \mathcal{H}_n^\ell(\mathbf{\Theta}_n^\ell, \beta, \delta; f, \boldsymbol{w})}{\partial \mathbf{\Theta}_n^\ell} =& m_1 \sum_{s \in \mathcal{B}_n^\ell} \delta_s P_n(s)^T \tilde{\boldsymbol{\nabla}} f(s) \left[\tilde{\boldsymbol{\nabla}} f(s)^T P_n(s) \mathbf{\Theta}_n^\ell + \tilde{f}_t(s) \right] \\ &+ \alpha\, m_2 \sum_{<s,r> \in \mathcal{C}_{\partial n}^\ell} \beta_{sr} P_n(s)^T \left[\boldsymbol{w}_s^\ell + P_n(s) \mathbf{\Theta}_n^\ell - \boldsymbol{w}_r \right] \\ &+ \alpha\, m_3 \sum_{<s,r> \in \mathcal{C}_n^\ell} \beta_{sr} (P_n(s) - P_n(r))^T \left[\boldsymbol{w}_s^\ell - \boldsymbol{w}_r^\ell + (P_n(s) - P_n(r)) \mathbf{\Theta}_n^\ell \right] = 0. \end{aligned} \tag{21}$$

A compact vectorial formulation of this equation can be achieved by introducing the following matrices and vectors indexed respectively by the sites of block $\mathcal{B}_n^\ell$, the cliques (i.e., interstitial sites) inside the block, and the cliques straddling the border of the block:

$$A_n \triangleq \begin{bmatrix} \vdots \\ \tilde{\boldsymbol{\nabla}} f(s)^T P_n(s) \\ \vdots \end{bmatrix}_{s \in \mathcal{B}_n^\ell}, \quad \boldsymbol{F}_n \triangleq \begin{bmatrix} \vdots \\ \tilde{f}_t(s) \\ \vdots \end{bmatrix}_{s \in \mathcal{B}_n^\ell}, \text{ and } \Delta_n \triangleq \mathrm{diag}(\cdots,\ \delta_s,\ \cdots)_{s \in \mathcal{B}_n^\ell},$$

$$C_n \triangleq \begin{bmatrix} \vdots \\ P_n(s) - P_n(r) \\ \vdots \end{bmatrix}_{<s,r> \in \mathcal{C}_n^\ell}, \text{ and } B_n \triangleq \mathrm{diag}(\cdots,\ \beta_{sr} \mathbb{I}_2,\ \cdots)_{<s,r> \in \mathcal{C}_n^\ell},$$

$$C_{\partial n} \triangleq \begin{bmatrix} \vdots \\ P_n(s) \\ \vdots \end{bmatrix}_{<s,r> \in \mathcal{C}_{\partial n}^\ell}, \text{ and } B_{\partial n} \triangleq \mathrm{diag}(\cdots,\ \beta_{sr} \mathbb{I}_2,\ \cdots)_{<s,r> \in \mathcal{C}_{\partial m}^\ell},$$

as well as the following block-wise and border-wise averages:

$$\overline{\mathbf{\Theta}}_{\partial n}^\ell \triangleq \frac{1}{b_{\partial n}} \sum_{<s,r> \in \mathcal{C}_{\partial n}^\ell} \beta_{sr} P_n(s)^T (\boldsymbol{w}_r - \boldsymbol{w}_s^\ell), \text{ with } b_{\partial n} \triangleq \sum_{<s,r> \in \mathcal{C}_{\partial n}^\ell} \beta_{sr}$$

$$\overline{\mathbf{\Theta}}_n^\ell \triangleq \frac{1}{b_n} \sum_{<s,r> \in \mathcal{C}_n^\ell} \beta_{sr} (P_n(s) - P_n(r))^T (\boldsymbol{w}_r^\ell - \boldsymbol{w}_s^\ell), \text{ with } b_n \triangleq \sum_{<s,r> \in \mathcal{C}_n^\ell} \beta_{sr}.$$

Linear equation (21) then reads:

$$\left[m_1 A_n^T \Delta_n A_n + \alpha m_2 C_{\partial n}^T B_{\partial n} C_{\partial n} + \alpha m_3 C_n^T B_n C_n \right] \mathbf{\Theta}_n^\ell = -m_1 A_n^T \Delta_n \boldsymbol{F}_n + \alpha m_2 b_{\partial n} \overline{\mathbf{\Theta}}_{\partial n}^\ell + \alpha m_3 b_n \overline{\mathbf{\Theta}}_n^\ell. \tag{22}$$

The direct resolution of this $p_n \times p_n$ linear system provides the updated value of parameter vector $\mathbf{\Theta}_n^\ell$. In this equation, matrices A_n, C_n and $C_{\partial n}$, and vectors $\overline{\mathbf{\Theta}}_n^\ell$ and $\overline{\mathbf{\Theta}}_{\partial n}^\ell$ depend on the type of parameterization associated with block $\mathcal{B}_n^\ell$. Let us give their expressions (when simplified forms are available) for the three levels of parameterization ($p_n = 2$, 4, and 6).

Constant model : In this case $P_n \equiv \mathbb{I}_2$, yielding $A_n^T = [\cdots \tilde{\boldsymbol{\nabla}} f(s) \cdots]_{s\in\mathcal{B}_n^\ell}$, $C_{\partial n}^T = [\cdots \mathbb{I}_2 \cdots]$, $C_n = 0$, $\overline{\boldsymbol{\Theta}}_n^\ell = 0$, and $\overline{\boldsymbol{\Theta}}_{\partial n}^\ell = \frac{1}{b_{\partial n}} \sum_{<s,r>\in\mathcal{C}_{\partial n}^\ell} \beta_{sr}(\boldsymbol{w}_r - \boldsymbol{w}_s^\ell)$. Equation (22) simplifies as follows:

$$
\begin{aligned}
(22) \quad &\Leftrightarrow \quad \left(m_1 A_n^T \Delta_n A_n + \alpha m_2 b_{\partial n} \mathbb{I}_2\right) \boldsymbol{\Theta}_n^\ell = -m_1 A_n^T \Delta_n \boldsymbol{F}_n + \alpha m_2 b_{\partial n} \overline{\boldsymbol{\Theta}}_{\partial n}^\ell \\
&\Leftrightarrow \quad \left(\frac{1}{\gamma} A_n^T \Delta_n A_n + \mathbb{I}_2\right) = \overline{\boldsymbol{\Theta}}_{\partial n}^\ell - \frac{1}{\gamma} A_n^T \Delta_n \boldsymbol{F}_n, \text{ with } \gamma \triangleq \alpha m_2 b_{\partial n} m_1 \\
&\Leftrightarrow \quad \boldsymbol{\Theta}_n^\ell = \overline{\boldsymbol{\Theta}}_{\partial n}^\ell - \frac{\gamma A_n^T \Delta_n (A_n \overline{\Theta}_{\partial n}^\ell + \boldsymbol{F}_n) + \det\mathbb{A}_n \overline{\boldsymbol{\Theta}}_{\partial n}^\ell + \mathrm{com}\mathbb{A}_n A_n^T \Delta_n \boldsymbol{F}_n}{\gamma(\gamma + \mathrm{tr}\mathbb{A}_n) + \det\mathbb{A}_n}, \text{ with } \mathbb{A}_n \triangleq \Delta_n A_n.
\end{aligned}
$$

Simplified affine model : In this case $P_n(s) = [\mathbb{I}_2 \; p(s)]$ with $p(s) \triangleq \begin{bmatrix} x_s & y_s \\ y_s & -x_s \end{bmatrix}$, yielding:

$$
\begin{aligned}
C_{\partial n}^T B_{\partial n} C_{\partial n} &= \sum_{<s,r>\in\mathcal{C}_{\partial n}^\ell} \beta_{sr} \begin{bmatrix} \mathbb{I}_2 & p(s) \\ p(s) & (x_s^2 + y_s^2)\mathbb{I}_2 \end{bmatrix} \\
C_n^T B_n C_n &= b_n \, \mathrm{diag}(0,0,1,1) \\
b_n \overline{\boldsymbol{\Theta}}_n^\ell &= \sum_{<s,r>\in\mathcal{C}_n^\ell(\vdots)} \beta_{sr} \begin{bmatrix} 1 & 0 \\ 0 & -1 \end{bmatrix} (\boldsymbol{w}_r^\ell - \boldsymbol{w}_s^\ell) + \sum_{<s,r>\in\mathcal{C}_n^\ell(\cdots)} \beta_{sr} \begin{bmatrix} 0 & 1 \\ 1 & 0 \end{bmatrix} (\boldsymbol{w}_r^\ell - \boldsymbol{w}_s^\ell),
\end{aligned}
$$

where $\mathcal{C}_n^\ell(\vdots)$ (resp. $\mathcal{C}_n^\ell(\cdots)$) contains cliques of $\mathcal{C}_n^\ell$ lying along the x-direction (resp. y-direction).

Affine model : In this case $P_n(s) = \mathbb{I}_2 \otimes \boldsymbol{e}(s)^T$, with $\boldsymbol{e}(s)^T \triangleq [1 \; x_s \; y_s]$, yielding the following expressions for the matrices and vectors involved in equation (22):

$$
\begin{aligned}
A_n^T \Delta_n A_n &= \sum_{s\in\mathcal{B}_n^\ell} \delta_s \left(\tilde{\boldsymbol{\nabla}} f(s) \tilde{\boldsymbol{\nabla}} f(s)^T\right) \otimes \left(\boldsymbol{e}(s)\boldsymbol{e}(s)^T\right) \\
C_{\partial n}^T B_{\partial n} C_{\partial n} &= \mathbb{I}_2 \otimes \sum_{<s,r>\in\mathcal{C}_{\partial n}^\ell} \beta_{sr} \boldsymbol{e}(s)\boldsymbol{e}(s)^T \\
C_n^T B_n C_n &= \mathbb{I}_2 \otimes \sum_{<s,r>\in\mathcal{C}_n^\ell} \beta_{sr} (\boldsymbol{e}(s) - \boldsymbol{e}(r))(\boldsymbol{e}(s) - \boldsymbol{e}(r))^T \\
&= \mathbb{I}_2 \otimes \mathrm{diag}\left(0, \sum_{<s,r>\in\mathcal{C}_n^\ell(\vdots)} \beta_{sr}, \sum_{<s,r>\in\mathcal{C}_n^\ell(\cdots)} \beta_{sr}\right) \\
A_n^T \Delta_n \boldsymbol{F}_n &= \sum_{s\in\mathcal{B}_n^\ell} \delta_s f_t(s) \tilde{\boldsymbol{\nabla}} f(s) \otimes \boldsymbol{e}(s) \\
b_{\partial n} \overline{\boldsymbol{\Theta}}_{\partial n}^\ell &= \sum_{<s,r>\in\mathcal{C}_{\partial n}^\ell} \beta_{sr} (\boldsymbol{w}_r - \boldsymbol{w}_s^\ell) \otimes \boldsymbol{e}(s) \\
b_n \overline{\boldsymbol{\Theta}}_n^\ell &= \sum_{<s,r>\in\mathcal{C}_n^\ell} \beta_{sr} (\boldsymbol{w}_r^\ell - \boldsymbol{w}_s^\ell) \otimes (\boldsymbol{e}(s) - \boldsymbol{e}(r)) \\
&= \sum_{<s,r>\in\mathcal{C}_n^\ell(\vdots)} \beta_{sr} (\boldsymbol{w}_r^\ell - \boldsymbol{w}_s^\ell) \otimes [0 \; 1 \; 0]^T + \sum_{<s,r>\in\mathcal{C}_n^\ell(\cdots)} \beta_{sr} (\boldsymbol{w}_r^\ell - \boldsymbol{w}_s^\ell) \otimes [0 \; 0 \; 1]^T.
\end{aligned}
$$

References

[1] G. ADIV. Determining three-dimensional motion and structure from optical flow generated by several moving objects. *PAMI*, 7:384–401, jul 1985.

[2] S. AYER and H.S. SAWHNEY. Layered representation of motion video using robust maximum-likelihood estimation of mixture models and MDL encoding. In *Proc. Int. Conf. Computer Vision*, pages 777–784, June 1995.

[3] J. BARRON, D. FLEET, and S. BEAUCHEMIN. Performance of optical flow techniques. *Int. J. Computer Vision*, 12(1):43–77, 1994.

[4] J.R. BERGEN, P. ANANDAN, K.J. HANNA, and R. HINGORANI. Hierarchical model-based motion estimation. In G. SANDINI, editor, *Proc. Europ. Conf. Computer Vision*, volume 558 of *LNCS-Series*, pages 237–252. Springer-Verlag, May 1992.

[5] M. BLACK and P. ANADAN. The robust estimation of multiple motions: parametric and piecewise-smooth flow fields. *Computer Vision and Image Understanding*, 63(1):75–104, 1996.

[6] M.J. BLACK and A. RANGARAJAN. On the unification of line processes, outlier rejection, and robust statistics with applications in early vision. *Int. Journ. of Comp. Vis*, 19(1):57–91, 1996.

[7] P. BOUTHEMY and E. FRANÇOIS. Motion segmentation and qualitative dynamic scene analysis from an image sequence. *Int. J. Computer Vision*, 10(2):157–182, 1993.

[8] P. CHARBONNIER, L. BLANC-FÉRAUD, G. AUBERT, and M. BARLAUD. Deterministic edge-preserving regularization in computed imaging. *IEEE Trans. Image Processing*, 3(1), 1996.

[9] I. COHEN and I. HERLIN. Optical flow and phase portrait methods for environmental satellite image sequences. In B. BUXTON and R. CIPOLLA, editors, *Proc. Europ. Conf. Computer Vision*, number 1064 in LNCS-Series, pages 141–150. Springer-Verlag, April 1996.

[10] R. DERICHE, P. KORNPROBST, and G. AUBERT. Optical flow estimation while preserving its discontinuities: a variational approach. In *Proc. Asian Conf. Computer Vision*, volume 1, pages 290–295, Singapore, December 1995.

[11] W. ENKELMANN. Investigation of multigrid algorithms for the estimation of optical flow fields in image sequences. *Comp. Vision Graph. and Image Proces.*, 43:150–177, 1988.

[12] D. GEMAN and G. REYNOLDS. Constrained restoration and the recovery of discontinuities. *IEEE Trans. Pattern Anal. Machine Intell.*, 14(3):367–383, 1992.

[13] S. GEMAN and D. E. McCLURE. Statistical methods for tomographic image reconstruction. In *Bull. ISI, Proc. 46th Session Int. Statistical Institute*, volume 52, 1987.

[14] F. HEITZ and P. BOUTHEMY. Multimodal estimation of discontinuous optical flow using Markov random fields. *IEEE Trans. Pattern Anal. Machine Intell.*, 15(12):1217–1232, 1993.

[15] F. HEITZ, P. PÉREZ, and P. BOUTHEMY. Multiscale minimization of global energy functions in some visual recovery problems. *CVGIP : Image Understanding*, 59(1):125–134, 1994.

[16] B.K.P. HORN and B.G. SCHUNCK. Determining optical flow. *Artificial Intelligence*, 17:185–203, 1981.

[17] M. IRANI, B. ROUSSO, and S. PELEG. Computing occluding and transparaent motions. *Int. J. Computer Vision*, 12(1):5–16, 1994.

[18] X. JU, M.J. BLACK, and A.D. JEPSON. skin and bones: multi-layer, locally affine, optical flow and regularization with transparency. In *Proc. Conf. Comp. Vision Pattern Rec.*, pages 307–314, 1996.

[19] J. KONRAD and E. DUBOIS. A comparison of stochastic and deterministic solution methods in bayesian estimation of 2D motion. In *Proc. First European Conference on Computer Vision*, pages 149–160, Antibes, France, apr 1990. Springer.

[20] Y. G. LECLERC. Constructing simple stable descriptions for image partitioning. *Int. Journ. of Computer Vision*, 3:73–102, 1989.

[21] E. MÉMIN and P. PÉREZ. Robust discontinuity-preserving model for estimating optical flow. In *Proc. Int. Conf. Pattern Recognition*, Vienna, Austria, August 1996.

[22] J.M. ODOBEZ and P. BOUTHEMY. Robust multiresolution estimation of parametric motion models. *Joun. of Vis. com. and Im. Repr.*, 6(4):348–365, 1995.

[23] M.T. ORCHARD. Predictive motion field segmentation for image sequence coding. *IEEE transaction on Circuits and Systems for video technology*, 3(1):54–70, Feb. 1993.

[24] M. PETROU, M. BOBER, and J. KITTLER. Multiresolution motion segmentation. In *Proc. Int. Conf. Pattern Recognition*, pages 379–383, Jerusalem, Israel, October 1994.

[25] P. PROESMANS, L. van GOOL, E. PAUWELS, and A. OOSTERLINCK. Determination of optical flow and its discontinuities using non-linear diffusion. In *Proc. Europ. Conf. Computer Vision*, volume 2, pages 295–304, Stokholm, Sweden, 1994.

[26] R. SZELISKI H.-Y. SHUM. Motion estimation with quadtree splines. In *Proc. Int. Conf. Computer Vision*, pages 757–763, 1995.

Unit´e de recherche INRIA Lorraine, Technopôle de Nancy-Brabois, Campus scientifique,
615 rue du Jardin Botanique, BP 101, 54600 VILLERS LÈS NANCY
Unit´e de recherche INRIA Rennes, Irisa, Campus universitaire de Beaulieu, 35042 RENNES Cedex
Unit´e de recherche INRIA Rhône-Alpes, 655, avenue de l'Europe, 38330 MONTBONNOT ST MARTIN
Unit´e de recherche INRIA Rocquencourt, Domaine de Voluceau, Rocquencourt, BP 105, 78153 LE CHESNAY Cedex
Unit´e de recherche INRIA Sophia-Antipolis, 2004 route des Lucioles, BP 93, 06902 SOPHIA-ANTIPOLIS Cedex

Éditeur
INRIA, Domaine de Voluceau, Rocquencourt, BP 105, 78153 LE CHESNAY Cedex (France)
http://www.inria.fr
ISSN 0249-6399